Inorg. Chem. **2008**, *47*, 2494−2506

On the Performance of Ligand Field Molecular Mechanics for Model Complexes Containing the Peroxido-Bridged $[Cu_2O_2]^{2+}$ Center

Christian Diedrich and Robert J. Deeth*

Inorganic Computational Chemistry Group, Department of Chemistry, University of Warwick, Coventry CV4 7AL, U.K.

Received September 13, 2007

The ability of ligand field molecular mechanics (LFMM) to model accurately the structures and relative conformer energies of complexes containing the $[Cu_2O_2]^{2+}$ unit found in oxidized copper type 3 (T3) enzymes is investigated. The consequences of ignoring the coupling between the metal centers are analyzed and predicted to be unimportant with respect to computing molecular geometries. Angular overlap model (AOM) parameters for the peroxido bridge in $[Cu_2O_2]^{2+}$ are derived on the basis of the mononuclear model compound $[(NH_3)_3CuO_2]$ for which good ligand field and density functional theory (DFT) calculations are also possible. Metal–ligand π-bonding parameters are shown to play an important role with the in-plane AOM π-bonding parameter value being significantly larger than that for the out-of-plane parameter. The LFMM treatment is then extended to the model dinuclear species $[(H_3N)_3CuO_2Cu(NH_3)_3]^{2+}$. The planarity of the $[Cu_2O_2]^{2+}$ moeity is implicitly obtained by defining the directions of the local Cu−O π-bonding interactions with respect to the other copper atom, rather than the other oxygen. In conjunction with the force field parameters based on the Merck molecular force field, the model, as implemented in our DommiMOE program (**Deeth, R. J.**; **Fey, N.**; **Williams-Hubbard, B. J.** *J. Comput. Chem.* 2005, *26*, 123–130), is applied to a set of crystallographically characterized small-molecule mimics of the T3 active site. Extensive LFMM conformational searches are carried out for these compounds, and the quality of the LFMM potential energy hypersurface is assessed by comparison with results using DFT. We find that the description of the geometries does not in fact suffer from the neglect of explicit coupling between the metal centers. Moreover, the structures and relative energies obtained by the LFMM conformational searches agree well with both experiment and the DFT values for all systems except one where the LFMM structure which is in best agreement with experiment is about 10 kcal mol^{-1} higher than the lowest energy conformer. However, this discrepancy is traced to generic shortcomings in the "organic" force field rather than the LFMM.

1. Introduction

Transition metal (TM) chemistry is crucially important for biological systems. Many enzymes owe their functionality to the chemical properties of their TM active sites[1] which often contain more than one metal center. Developing a good, molecular-level understanding of the structure–function relationship in such systems is challenging. Alongside the plethora of powerful spectroscopic techniques available,[2] it is important to be able to employ theoretical models. However, TM systems of biochemical relevance still pose many problems for computational chemistry. Although the electronic structure of the active site itself can often be rationalized with the help of density functional theory (DFT), time-resolved investigations of the complete systems by means of molecular dynamics (MD) simulations require an appropriate empirical force field (FF). Despite the many successful applications of molecular mechanics to relatively

* To whom correspondence should be addressed. E-mail: r.j.deeth@warwick.ac.uk.

(1) Kaim, W.; Schwederski, B. *Bioinorganic Chemistry: Inorganic Elements in the Chemistry of Life*; John Wiley and Sons: Chichester, 1994.
(2) Solomon, E. I.; Szilagyi, R. K.; George, S. D.; Basumallick, L. *Chem. Rev.* **2004**, *104*, 419–458.
(3) Comba, P.; Hambley, T. W. *Molecular Modelling of Inorganic Compounds*; Wiley-VCH: Weinheim, 1995.
(4) Bernhardt, P. V.; Comba, P. *Inorg. Chem.* **1992**, *31*, 2638–2644.
(5) Bernhardt, P. V.; Comba, P.; Hambley, T. W.; Massoud, S. S.; Stebler, S. *Inorg. Chem.* **1992**, *31*, 2644–2651.
(6) Adam, K. R.; Antolovich, M.; Bridgen, L. G.; Lindoy, L. F. *J. Am. Chem. Soc.* **1991**, *113*, 3346–3351.

10.1021/ic701803g CCC: $40.75
Published on Web 02/23/2008

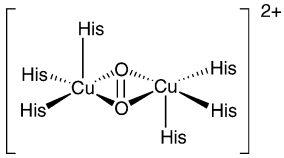

Figure 1. Copper type 3 center active site (His = histidine).

small TM complexes,[3–11] the description of complexes with stereochemically active d electrons is limited within the conventional FF approaches usually used for biochemical simulations.

We have recently shown for copper type 1 enzymes[12,13] that ligand field molecular mechanics (LFMM)[14] represents a very promising candidate for filling this gap. In the framework of this hybrid method, which is computationally competitive with standard FFs, the electronic effects of the d-electrons are automatically built into the model by combining classical FF terms with a ligand field stabilization energy contribution obtained from the angular overlap model (AOM).[15–18] However, in its original form, the AOM is essentially a localized theory based on the assumption of single, separated metal centers. Hence, it is not a priori clear to what extent LFMM is applicable to the multimetal systems in the active sites of many metalloproteins. This prompted us to undertake the present "proof of concept" study.

An interesting class of multimetal enzymes is characterized in its fully oxidized state by a dinuclear side-on peroxido-bridged copper cluster (Figure 1) which is usually referred to as copper type 3 (T3) center. Examples are hemocyanin, the oxygen storage protein of molluscs and arthropods,[19,20] catechol oxidase,[21] and tyrosinase,[22] all of which exhibit remarkably similar active sites despite their entirely different protein structures.

A series of small, model compounds for the T3 center has been synthesized over the past 10 years in order to mimic the reversible oxygen binding capability of the enzyme.[23–27] These molecules contain multidentate N-donor chelate ligands which retain the main structural features present in the enzymes. That is, the arrangement of the ligand atoms around the metal center is not only influenced by the nature of the ligands and the electron configuration of the metal but also by the preorganization of the donor atoms. In this work, we focus on four of these model compounds for which high-resolution crystal structures are available[23–27] and which are also small enough to allow full DFT geometry optimizations to aid the derivation and validation of the LFMM parameters.

Two of these complexes (**I** and **II**) have closely related hexadentate ligands which connect the two tridentate pyridyl units by an ethylene bridge. Despite the similarity of these two compounds, we include both since DFT predicts subtly different structures which highlight the difficulties of capturing in a theoretical model the delicate balance between the strain imposed by the chelate ligand and the Jahn–Teller (J−T) distortions in these systems which are sensitive to seemingly minor structural details. [Strictly speaking, a Jahn–Teller distortion requires a degeneracy of at least two electronic states which is not present here. However, the unequal copper−nitrogen bond lengths in these systems have essentially the same physical origin as a Jahn–Teller elongation, namely the (near) degeneracy of different electronic states, which results in a conical intersection between the two corresponding Born–Oppenheimer hypersurfaces. For the sake of convenience we will therefore use the terms Jahn–Teller distortion and Jahn–Teller axis throughout this paper.] The compounds **III** and **IV** in Figure 2 do not contain a link between the metal sites other than the peroxido bridge, but the steric demands of the respective ligands still result in significant strain in the molecular system.

In this paper we derive angular overlap model (AOM) parameters for the peroxido ligand in copper T3 centers and present LFMM and DFT geometry optimizations for different conformers of the four model compounds derived from LFMM stochastic conformational searches. The ability of LFMM and DFT to reproduce the experimental geometries is critically investigated. Then, we will briefly discuss the electronic structure of the copper T3 centers and give an outline of the AOM with the emphasis on dinuclear complexes. Following the computational details section, the LFMM results for the model compounds will be discussed.

2. Theory

2.1. Electronic Structure of the Copper Type 3 Center. The electronic structure of the copper T3 center has been extensively analyzed with various quantum chemical methods of different levels of accuracy. The main focus of most of these studies has been the relative energies of the peroxido side-on bound form of the copper site compared

(7) Hay, B. P. *Coord. Chem. Rev.* **1993**, *126*, 177–236.
(8) Comba, P.; Hambley, T. W.; Zipper, L. *Helv. Chim. Acta* **1988**, *71*, 1875–1880.
(9) Hambley, T. W. *Inorg. Chem.* **1988**, *27*, 1073–1077.
(10) Hambley, T. W. *J. Chem. Soc., Dalton Trans.* **1986**, 565–569.
(11) Hancock, R. D.; Dobson, S. M.; Evers, A.; Wade, P. W.; Ngwenya, M. P.; Boeyens, J. C. A.; Wainbright, K. P. *J. Am. Chem. Soc.* **1988**, *110*, 2788–2794.
(12) Deeth, R. J. *Chem. Commun.* **2006**, *24*, 2551–2553.
(13) Deeth, R. J. *Inorg. Chem.* **2007**, *46*, 4492–4503.
(14) Burton, V. J.; Deeth, R. J.; Kemp, C. M.; Gilbert, P. J. *J. Am. Chem. Soc.* **1995**, *117*, 8407–8415.
(15) Schäffer, C. E.; Jørgensen, C. K. *Mol. Phys.* **1965**, *9*, 401–412.
(16) Woolley, R. G. *Mol. Phys.* **1981**, *42*, 703–720.
(17) Gerloch, M.; Woolley, R. G. *Prog. Inorg. Chem.* **1983**, *31*, 371–446.
(18) Richardson, D. E. *J. Chem. Educ.* **1993**, *70*, 372–380.
(19) Hazes, B.; Magnus, K. A.; Bonaventura, C.; Bonaventura, J.; Dauter, Z.; Kalk, K. H.; Hol, W. G. *Protein Sci.* **1993**, *2*, 597–619.
(20) Magnus, K. A.; Hazes, B.; Ton-That, H.; Bonaventura, C.; Bonaventura, J.; Hol, W. G. *Proteins* **1994**, *19*, 302–309.
(21) Gerdemann, C.; Eiken, C.; Krebs, B. *Acc. Chem. Res.* **2002**, *35*, 183–191.
(22) Matoba, Y.; Kumagai, T.; Yamamoto, A.; Yoshitsu, H.; Sugiyama, M. *J. Biol. Chem.* **2006**, *281*, 8981–8990.
(23) Kodera, M.; Katayama, K.; Tachi, Y.; Kano, K.; Hirota, S.; Fujinami, S.; Suzuki, M. *J. Am. Chem. Soc.* **1999**, *121*, 11006–11007.
(24) Kodera, M.; Kajita, Y.; Tachi, Y.; Katayama, K.; Kano, K.; Hirota, S.; Fujinami, S.; Suzuki, M. *Angew. Chem., Int. Ed.* **2004**, *43*, 334–337.
(25) Kitajima, N.; Fujisawa, K.; Moro-oka; Toriumi, K. *J. Am. Chem. Soc.* **1989**, *111*, 8975–8976.
(26) Kitajima, N.; Fujisawa, K.; Fujimoto, C.; Moro-oka, Y.; Hashimoto, S.; Kita- gawa, T.; Toriumi, K.; Tatsumi, K.; Nakamura, A. *J. Am. Chem. Soc.* **1992**, *114*, 1277–1291.
(27) Lam, B. M. T.; Halfen, J. A.; Young, V. G., Jr.; Hagadorn, J. R.; Holland, P. L.; Lledos, A.; Cucurull-Sanchez, L.; Novoa, J. J.; Alvarez, S.; Tolman, W. B. *Inorg. Chem.* **2000**, *39*, 4059–4072.

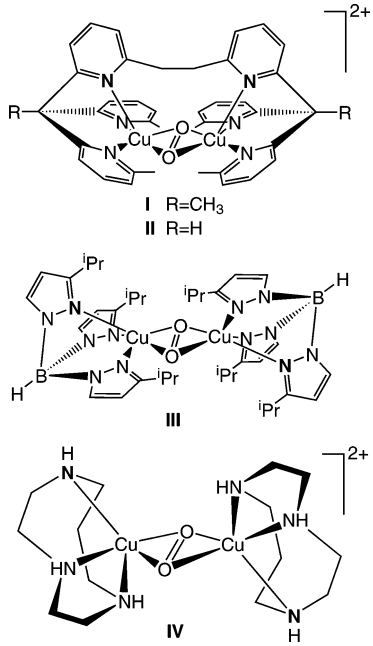

Figure 2. Copper type 3 center model compounds: **I**, ref 23; **II**, ref 24; **III**, refs25 and 26; **IV**, ref 27. The longer Cu−N bonds are identified by a bond N.

to the corresponding oxo structure.[27–32] Since the peroxido nature of the oxidized T3 center has now been established by spectroscopic and crystallographic evidence (see ref 33 for an overview), we will not deal with the two isomers of the $[Cu_2O_2]^{2+}$ unit in this paper. Nevertheless, one important conclusion of the previous computational studies is important to mention here: the varying degrees of dynamic and static correlation in the wave function, as well as the different balance between covalent and ionic bonding in the different copper oxygen binding modes, severely hamper their accurate computational treatment. In particular, the accuracy of density functional theory (DFT) is significantly influenced such that even DFT predictions for the molecular geometries, which for the majority of "normal" metal complexes compare favorably with experiment, have to be considered less reliable for the present systems.

Many of the computational studies in the literature are based on the C_{2h} symmetric model compound $[(NH_3)_3CuO_2Cu(NH_3)_3]^{2+}$ (PO) which captures the main electronic and structural features of the T3 center and therefore represents a reasonable test system for computational methods. It is therefore an obvious starting point for the parametrization of the LFMM. However, the AOM in its original form is a single-metal-center model which relies on the fact that in many Werner-type complexes the antibonding energy of the d orbitals is dominated by the interaction only with the atoms directly bound to the metal. It is not a priori clear to what extent the model needs to be modified for multimetal systems in order to describe sufficiently accurately our main quantities of interest, namely the molecular geometry and relative conformer energy.

2.2. LFMM for Peroxido-Bridged Dinuclear Complexes. 2.2.1. General Considerations. The basic assumption of the extended AOM model[34–36] is that the separated treatment of the two metal centers essentially remains valid and therefore can be described by means of the single-center AOM model plus a "correction" which accounts for the coupling between the metal centers through the bridging ligands. That is, the starting point for a generalization to dinuclear complexes is an eigenvalue equation of the form

$$[\hat{V}^{A} + \hat{V}^{B} + \hat{V}^{AB}]\Psi_I^{AB} = \epsilon_I^{AB}\Psi_I^{AB} \quad (1)$$

where V^A and V^B correspond to the usual single center AOM operators and V^{AB} determines the strength of the coupling between the two metal centers. Originally, the extension of the AOM to dinuclear systems was proposed by Glerup[34] without giving explicit expressions for the operator V^{AB}. It has been improved by various authors[35,36] and further extended and reviewed by Schäffer in 2000.[37] Although this ansatz for the dinuclear AOM operator (eq 1) preserves the main idea of the single-center AOM, there is a very important difference: the reference "ligand field" system for the dinuclear complex is no longer spherically symmetric but features $D_{\infty h}$ symmetry. Hence, the atomic orbital basis set of d orbitals centered on the metal atoms does not have the correct symmetry to form eigenfunctions of the one-electron overall ligand field operator $V^T = \hat{V}^A + \hat{V}^B + \hat{V}^{AB}$. Symmetry adaption yields a set of 10 functions of the general form

$$\Psi_I^{AB} = \sum_i^5 c_i\varphi_i^A \pm \sum_j^5 c_j\varphi_j^B \quad (2)$$

That is, each pair of single-center eigenfunctions φ^A and φ^B is replaced by the linear combinations $\varphi^A + \varphi^B$ and $\varphi^A - \varphi^B$, one of which is of gerade and one of which is of ungerade symmetry. At this point, it is important to note that without any bridging ligands the splitting between the gerade and ungerade combinations of the d levels is negligibly small and does not need further consideration. This implies that significant splitting can only occur for d orbitals with the right orientation with respect to the bridging ligands. Furthermore, if one were to parametrize the model for a 10-orbital basis set, the interaction between a given gerade d orbital combination and a particular ligand orbital can be very different from the corresponding ungerade combination. For example, a p orbital in a linear bridging ligand cannot

(28) Cramer, C. J.; Wloch, M.; Piecuch, P.; Puzzarini, C.; Gagliardi, L. *J. Phys. Chem. A* **2006**, *110*, 1991–2004.
(29) Rode, M. F.; Werner, H.-J. *Theor. Chim. Acta* **2005**, *114*, 309–317.
(30) Liu, X.-Y.; Palacios, A. A.; Novoa, J. J.; Santiago, A. *Inorg. Chem.* **1998**, *37*, 1202–1212.
(31) Siegbahn, P. E. M. *Faraday Discuss.* **2003**, *124*, 289–296.
(32) Henson, M. J.; Mukherjee, P.; Root, D. E.; Stack, T. D. P.; Solomon, E. I. *J. Am. Chem. Soc.* **1999**, *121*, 10332–10345.
(33) Solomon, E. I.; Sundaram, U. M.; Machonkin, T. E. *Chem. Rev.* **1996**, *96*, 2563–2606.
(34) Glerup, J. *Acta Chem. Scand.* **1972**, *26*, 3775–3787.
(35) Bencini, A.; Gatteschi, D. *Inorg. Chim. Acta* **1978**, *31*, 11–18.
(36) Weihe, H.; Güdel, H. U. *J. Am. Chem. Soc.* **1998**, *120*, 2870–2879.
(37) Schäffer, C. E. *Inorg. Chim. Acta* **2000**, *1035*, 300–302.

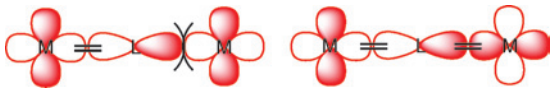

Figure 3. Interaction of a p orbital of a linear bridging ligand with gerade (left-hand side) and ungerade d orbital combinations. Bonding and antibonding interactions are indicated by double straight lines and circle arcs, respectively. The net M−L interaction for the left-hand figure is thus exactly zero.

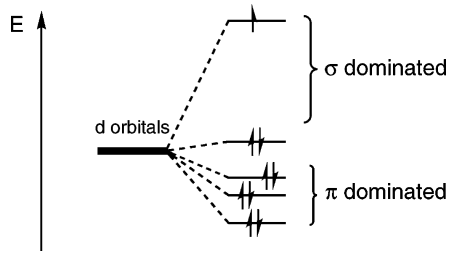

Figure 4. Electrostatic approach to ligand field theory: d orbitals split up as a result of the electrostatic repulsion with the ligand orbitals.

interact with gerade d orbital combinations, whereas interaction with the corresponding ungerade orbital can potentially be very strong (see Figure 3).

2.2.2. Relevance for Copper T3 Centers. As mentioned, our main focus in this work is on the molecular geometry and the energy differences induced by conformational changes rather than spectroscopic or magnetic properties. Therefore, from a purely pragmatic point of view, we intend to treat the metal centers in the T3 $[Cu_2O_2]^{2+}$ cluster "as locally as possible" such that additional parameters for the metal−metal coupling are avoided. This will only be acceptably accurate if the influence of the coupling on the gradient with respect to the energy is small. We will see that there is a high probability that this is indeed the case.

Consider first the gradient of the barycentered LFSE of an isolated Cu(II) system:

$$\frac{\partial E^{\mathrm{LFSE}}}{\partial r} = \frac{\partial}{\partial r}\left[\sum_{j=1}^{5} n_j\left(\epsilon_j - \frac{1}{5}\sum_{i=1}^{5}\epsilon_i\right)\right] \tag{3}$$

For a d^9 configuration the occupation numbers n_j are 2 for $1 \le j \le 4$ and 1 for $j = 5$. Inserting this into eq 3 yields after rearranging

$$\frac{\partial E^{\mathrm{LFSE}}}{\partial r} = \frac{\partial}{\partial r}\left[2\sum_{j=1}^{4}\left(\epsilon_j - \frac{1}{5}\sum_{i=1}^{5}\epsilon_i\right) + \epsilon_5 - \frac{1}{5}\sum_{i=1}^{5}\epsilon_i\right] = \left[-\frac{4}{5}\frac{\partial}{\partial r}\epsilon_5 + \frac{1}{5}\sum_{j=1}^{4}\frac{\partial}{\partial r}\epsilon_j\right] \tag{4}$$

that is, as a result of the bary-centering, the gradient of the energy of the singly occupied orbital represents the dominant contribution in the total gradient. Consequently, the geometry will be rather sensitive to the parameters which influence the energy of the highest d orbital whereas the response to parameters which mainly influence the doubly occupied orbitals will be less pronounced. This result correlates with the ligand-field picture (see Figure 4) which associates the high-energy d orbitals mainly with stronger M−L σ interactions while the lower energy d orbitals are mainly of M−L π symmetry.

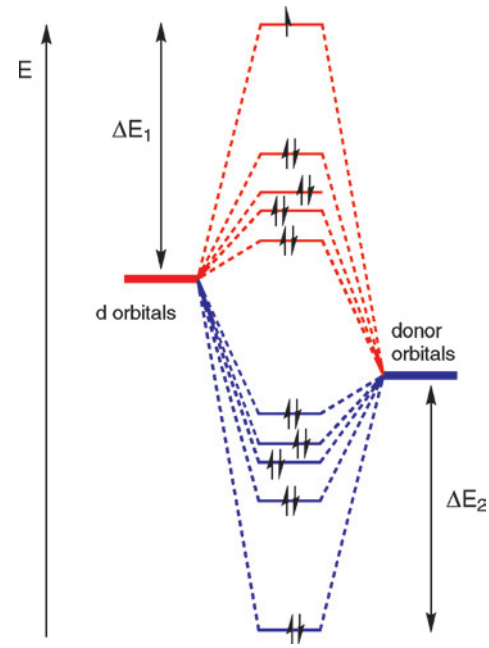

Figure 5. MO interpretation of d-electron stabilization energy in d^9 complexes. Any d-like orbitals (red) which are doubly occupied have a small effect on the overall energy since any changes in energy are countered by equal and opposite changes in the corresponding bonding MO (blue). In contrast, the stabilizing effect of the singly occupied orbital is $\Delta E_1 - 2\Delta E_2$.

An alternative rationalization can also be formulated in simple molecular orbital (MO) terms as described, for example, by Burdett.[38] In the MO model, each AOM antibonding d orbital has a corresponding bonding function localized mainly on the ligands. To a first approximation, the energy change of a doubly occupied AOM orbital is thus canceled by an equal but opposite energy change of the corresponding doubly occupied bonding function. Hence, doubly occupied AOM orbitals have a relatively weak effect on the total energy of the overall system. For a singly occupied AOM orbital, on the other hand, the doubly occupied ligand-based bonding MO exerts a strongly stabilizing effect on the molecule (see Figure 5). Consequently, for mononuclear Cu(II) systems special attention should be paid to the energy of the highest orbital relative to the average of the other ones when deriving AOM parameters for use with LFMM. The LFSE is less sensitive with respect to moderate energy changes among the doubly occupied orbitals.

These considerations can readily be extended to the case of copper T3 centers where the effect of metal−metal coupling through the ligand orbitals, as sketched above, may need to be taken into account. Consider the bary-centered LFSE in the 10-orbital basis set (eq 2):

$$E^{\mathrm{LFSE/10d}} = \sum_{j=1}^{10} n_j\left(\epsilon_j^{\mathrm{10d}} - \frac{1}{10}\sum_{i=1}^{10}\epsilon_i^{\mathrm{10d}}\right) \tag{5}$$

For a $[Cu(II)O_2Cu(II)]^{2+}$ 18-electron system, one obtains nine doubly occupied and one empty orbital which, by the same

(38) Burdett, J. K. *Molecular Shapes: Theoretical Models of Inorganic Stereochemistry*; Wiley: New York, 1980.

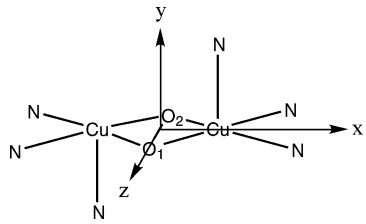

Figure 6. Orientation of the Cartesian axis frame for the PO model system, $[(NH_3)_3CuO_2Cu(NH_3)]^{2+}$.

Table 1. Fragment Orbitals for the $[Cu_2O_2]^{2+}$ Unit in C_{2h}

d orbital	irrep (C_s)[a]	comb	irrep (C_{2h})	O_2^{2-} MO[b]	AOM parameter[c]
$\mathbf{d_{x^2-y^2}}$	a′	+	a_g	σ	e_σ, $e_{\pi\|}$
		−	b_u	π_x, $(\pi_y)^d$	e_σ, $e_{\pi\|}$
d_{z^2}	a′	+	a_g	σ	—[e]
		−	b_u	π_x, π_y	—[e]
$\mathbf{d_{xy}}$	a′	+	a_g	$(\sigma)^d$	$e_{\pi\perp}$
		−	b_u	(π_x),[d] π_y	$e_{\pi\perp}$
$\mathbf{d_{xz}}$	a″	+	b_g	π_x*, $(\pi_y$*$)^d$	e_σ, $e_{\pi\|}$
		−	a_u	σ*	e_σ, $e_{\pi\|}$
d_{yz}	a″	+	b_g	π_x*, π_y*	—[e]
		−	a_u	σ*	—[e]

[a] Irreducible representation in C_s (local symmetry on each copper center). [b] Orbital labels refer to the orientation of PO given in Figure 6. [c] $\pi_{\|}$: π-bonding in the CuOO plane; $\pi_\perp$: π-bonding perpendicular to CuOO plane. [d] Overlap close to zero because of spatial orientation. [e] Interaction is comparatively weak. Fragment orbitals for the $[Cu_2O_2]^{2+}$ unit in C_{2h}.

argument as for a single Cu(II) center (eq 4), yields the gradient of the LFSE:

$$\frac{\partial E^{\mathrm{LFSE/10d}}}{\partial r} = 2\left(-\frac{9}{10}\frac{\partial}{\partial r}\epsilon_{10} + \frac{1}{10}\sum_{j=1}^{9}\frac{\partial}{\partial r}\epsilon_j\right) \qquad (6)$$

In light of our initial idea to neglect as much of the metal−metal coupling as possible, this is a very convenient result. If we consider the full 10d problem, the orbital energies and the respective contributions to the gradient of the nine occupied orbitals are scaled down by a factor of 1/10. This, of course, is also true for errors in these energies. In other words, if the splitting between the corresponding $d_{nm} + d_{nm}$ and $d_{nm} - d_{nm}$ combinations is moderate, there is a very good chance of obtaining a decent description of the molecular geometry and of the total energy of the system even when the coupling is ignored—which essentially means setting $\epsilon(d_{nm} + d_{nm}) = \epsilon(d_{nm} - d_{nm})$. One requirement, however, remains crucial: the energy of the empty orbital (ϵ_{10}) relative to the average of the other ones needs to be described reasonably well.

Qualitatively, basic MO theory considerations confirm this. Assuming the orientation of PO given in Figure 6, the fragment orbitals of the Cu−Cu and the O_2^{2-} subunits in $[Cu_2O_2]^{2+}$ are obtained as summarized in Table 1. The d orbitals predominantly influenced by the O_2^{2-} bridge are highlighted in bold. As a result of our calculated comparatively small O−Cu−O angle of ≈42°, the interaction with the d_{z^2} and the d_{yz} orbital is relatively weak, and their orbital energies are mainly influenced by the nonbridging ligands.

Out of the three remaining d orbitals (that is, six in-phase and out-of-phase combinations), by chemical intuition one of the d_{xz} orbital combinations can be expected to have the highest energy since this orbital points toward the corners

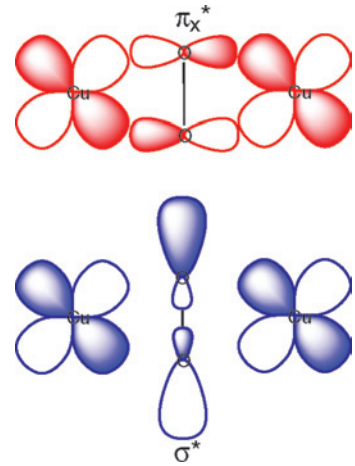

Figure 7. Bonding combination of $d_{xz} + d_{xz}$ and π_x* orbital as well as $d_{xz} + d_{xz}$ and σ*. Axis frame is as defined in Figure 6.

of the pseudoplane in which the peroxido bridge and the equatorial nitrogen ligands lie. The $d_{yz}-d_{yz}$ orbital only interacts with the σ* orbital whereas the plus combination has the correct symmetry (see Table 1) for mixing with the π_x* orbital which has an ideal spatial orientation for maximum overlap (see Figure 7). The bonding (ligand based) combination of these two orbitals can therefore be expected to be very low in energy which implies a very high energy of the antibonding (metal-based) combination. These considerations are indeed confirmed by our DFT calculations.

In a hypothetical mononuclear peroxido complex, there is only one d_{xz} orbital, and it can interact with both the σ* and the π_x* orbital. However, for analogous reasons to those given above, the influence will mainly be dominated by π_x*. That is, if the AOM is parametrized for a mononuclear peroxido model complex, there is good reason to believe that the set of e_σ and $e_{\pi\|}$ parameters derived on this basis will provide a reasonable description for the $d_{xz} + d_{xz}$ orbital as well. This conclusion, in combination with the implications of eq 6, suggests that no additional coupling parameters are needed for a reasonable description of the geometry of a copper T3 center. We are aware that this derivation does not represent an extension of the AOM in a theoretically complete sense. It does, however, form the basis for the extension of the LFMM for copper-containing multimetal systems. Whether or not these results are generalizable to other metals will be investigated further in the future.

2.2.3. Derivation of AOM Parameters for O_2^{2-}. The typical procedure for deriving AOM parameters is to set up a reference system with a symmetry high enough to distinguish between the d levels. For mononuclear complexes, d orbital energies can then be obtained from DFT average over configurations (AOC)[39] calculations and used to fit appropriate AOM parameters. This procedure is not applicable here because the reference system (PO) is only C_{2h} symmetric and contains two metal centers. An obvious consequence of the dinuclear nature of the complex is that a DFT calculation yields a set of 10 d orbital combinations

(39) Anthon, C.; Bendix, J.; Schäffer, C. E. *Inorg. Chem.* **2003**, *42*, 4088–4097.

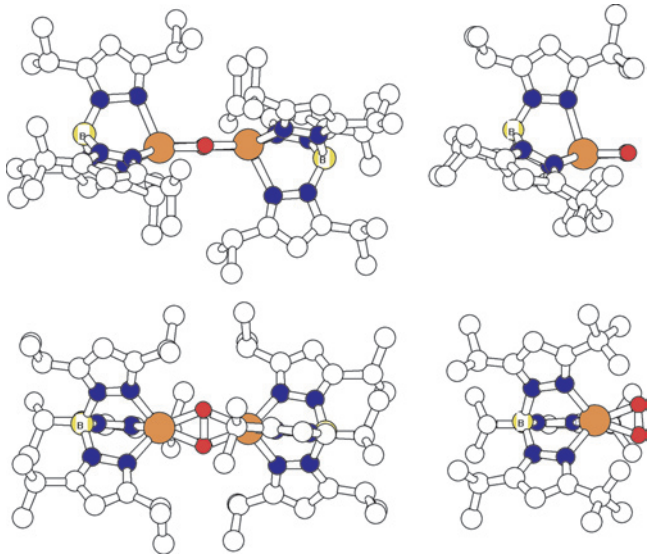

Figure 8. Comparison of dinuclear and mononuclear copper−peroxido complexes based on **III**.

Table 2. Comparison of Cu−N Bond Lengths (in Å) and Angles (in deg) in Compound **III** and Its Mononuclear Derivative[40]

	mononuclear (C_s)[a]		binuclear (C_s)[b]	
atoms	R^c	$\angle^d$	R^c	$\angle^d$
N_{ax}−Cu	2.25	−74.3	2.26	−65.1
R(N_{eq}−Cu)	1.99	12.2	1.99//2.00	17.4//12.0
R(O−Cu)	1.84		1.90//1.93	

[a] Reference 40. [b] References 25 and 26. [c] Bond lengths (in Å) between atoms given in first column. [d] Angles (in deg) between CuOO plane and bond vectors of atoms given in first column.

(eq 2) which is not directly transferable to our purely localized AOM scheme. Various averaging schemes have been tested to reduce the ten DFT d orbital energies to a "localized" set of five orbitals, but none is very satisfactory, partly because the averaging always contains an element of arbitrariness and partly because of the overly delocalized DFT description of the complex.

For these reasons, we decided to use a mononuclear model complex for deriving the AOM parameters. This procedure seems justified since despite the bridging ligand, the two copper centers still feature many of the properties of isolated copper complexes. For example, compound **III** has a mononuclear derivative[40] with a very similar geometry around the metal center to each half of the complete system (Figure 8 and Table 2). The data shown in Table 2 refer to the angles between the Cu−peroxido plane and the respective bond axes as shown in Figure 9 and describe the deviation from idealized planar geometry. Different signs imply ligands on different sides of the Cu−peroxido plane. We will use these angles in combination with the respective bond lengths to characterize the geometries throughout this paper.

An obvious choice for a mononuclear reference system is "one-half" of PO. In addition to cutting off the second metal

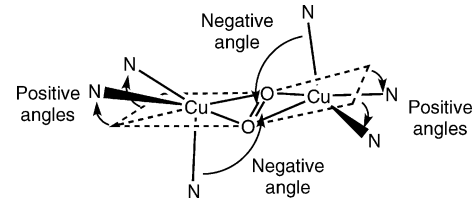

Figure 9. Angle definitions for Cu−N coordination.

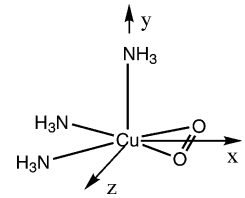

Figure 10. Mononuclear analogue of PO (MNPO). Orientation of the Cartesian axes adopted from PO.

Table 3. Relative d Orbital Energies of MNPO Obtained by DFT and CAMMAG

irrep in C_s	orbital	DFT[a,b]	AOM[a]
a″	d_{xz}	25004.6	25947.7
a′	$d_{x^2-y^2}$	7735.3	7893.0
a′	d_{z^2}	4266.9	4318.7
a′	d_{xy}	2694.0	2494.0
a″	d_{yz}	0.0	0.0

[a] Energy in cm^{-1}. [b] AOC calculation; see theory section.

center, the equatorial nitrogen ligands were bent into the CuO_2 plane and the N−Cu−N angle was adjusted to 90° (see Figure 10). This of course does not change the actual symmetry, but it reduces the mixing between the d levels without affecting the orbital energy pattern very much. This facilitates the assignment of the orbitals obtained from DFT calculations. This slight change in the geometry does not change the main features of the ligand field such that the AOM parameters derived on this basis are expected to be equally valid for the corresponding equilibrium geometry. Note that the LFSE only contributes one part of the total LFMM potential energy hypersurface, and the distortion away from the square-planar arrangement is accounted for by the ligand−ligand repulsion (see ref 41), which of course is unaffected by the way the AOM parameters are derived.

The AOC calculation has been carried out using the Amsterdam Density Functional program (see computational details section). In order to compensate for the tendency of DFT to generally overestimate covalency,[42] the copper nuclear charge has been reduced by 0.8 while the COSMO solvent model[43] was used to obtain a better balance between the relative covalencies of N and O donors.[44] The relative d orbital energies obtained in this way are summarized in Table 3. As expected, the mononuclear compound also has the d_{xz} orbital highest in energy. The big gap between this orbital and the remaining ones is noticeable and according to eq 5 results in a large LFSE. In order to find suitable AOM parameters for O_2^{2-} which, in combination with the nitrogen

(40) Fujisawa, K.; Tanaka, M.; Moro-oka, Y.; Kitajima, N. *J. Am. Chem. Soc.* **1994**, *116*, 12079–12080.
(41) Deeth, R. J.; Fey, N.; Williams-Hubbard, B. *J. Comput. Chem.* **2004**, *26*, 123–130.
(42) Deeth, R. J. *Dalton Trans.* **2001**, 664–669.
(43) Klamt, A.; Schüürmann, G. *J. Chem. Soc., Perkin Trans. 2* **1993**, 799–805.
(44) Hocking, R. K.; Deeth, R. J.; Hambley, T. W. *Inorg. Chem.* **2007**, *46*, 8238–8244.

Table 4. Comparison of DFT and LFMM Geometries of PO

	DFT[a]		LFMM	
atoms	R^b	$\angle^c$	R^b	$\angle^a$
$Cu-N_{ax}$	2.23	−81.5	2.26	−83.4
$Cu-N_{eq}$	2.05	18.3	2.05	13.3
Cu−O	2.00		1.95	

[a] Technical details in computational details section. [b] Bond lengths (in Å) between atoms given in first column. [c] Angles (in deg) between CuOO plane and bond vectors of atoms given in first column.

parameters from our library reproduce the DFT orbital energies, a series of CAMMAG[45,46] calculations has been carried out. The values obtained with the "best-fit" AOM parameters are remarkably similar to the DFT ones (Table 3).

As a first obvious test for the new AOM parameters, a LFMM geometry optimization for PO has been carried out. This compound also served as a starting point for calibrating the Morse parameters and the ligand−ligand repulsion parameters to complete the LFMM parameter set (see ref 41 for a detailed description of our parametrization). Table 4 shows that with the adjusted parameters the geometry of PO is well reproduced. Note that the same bond stretching parameters are used for equatorial and axial nitrogens. Clearly, the LFMM is capable of describing the elongated apical bonds of the two copper centers in PO satisfactorily.

Apart from these elongations, the planar $[Cu_2O_2]^{2+}$ core is a very important geometrical feature. Planarity is achieved by using the strongly asymmetrical π-bonding parameters for the peroxido ligand derived from our mononuclear model compound ($e_{\pi\parallel} \gg e_{\pi\perp}$) with an additional crucial feature. In the mononuclear model system, the local Cu−O axis frame is defined using the other oxygen atom. For the dinuclear species, the local axis frame is defined using the other copper atom. Thus, any "folding" about the O−O axis rotates the local x and y axes which define the $e_{\pi\parallel}$ and $e_{\pi\perp}$ directions. Folding to 90° would actually interchange the π-bonding directions.

One of the originally conceived advantages of the LFMM over conventional MM was the ability to treat separately the individual effects of M−L σ and π bonding.[14] Here is the first application which demonstrates a definitive role for M−L π parameters. Moreover, $e_{\pi\parallel} \gg e_{\pi\perp}$ seems entirely consistent with simple ligand field arguments. The valence orbitals on the peroxido ligand are the originally degenerate π-antibonding MOs. The in-plane π^* orbital interacts strongly, and in a more-or-less σ sense, with d_{xz} ($e_{\pi\parallel}$ large) while the out-of-plane π^* orbital interacts less strongly because it is of π symmetry with respect to Cu−O bonding ($e_{\pi\perp}$ small).

The maximum LFSE thus occurs when the $[Cu_2O_2]^{2+}$ unit is completely flat. This is illustrated in Figure 11, which displays how the d orbital energies change upon folding about the OO axis. The predominant effect is a pronounced decrease of the d_{xz} orbital energy with respect to the other four d orbitals. Because of the d^9 configuration, the change of the highest energy d orbital equals the change in LFSE, and therefore, the LFSE provides maximum stabilsation for $\alpha = 180°$. The definition of the asymmetric π-bonding directions on one particular copper center using the other copper atom couples the two ligand systems in a way which, empirically, is satisfactory for a proper description of the geometry of the system. The correct geometry is thus implicit in the model without adding explicit FF terms to penalize distortion out of the copper−peroxido plane.

Following our general strategy for deriving LFMM parameters for heteroleptic systems on the basis of suitable homoleptic reference systems,[13] the remaining parameters for the nitrogen donors have been taken from our library. This is based on the reasonable assumption that, from the nonbridging ligands' perspective, the individual metal centers behave very similarly to their mononuclear equivalents.

With the LFMM parameter set completed the quest for a suitable parent FF arises. The LFMM approach is designed for easy incorporation into any conventional FF distributed with MOE (see below). Since our ultimate goal is the description of copper T3 enzymes, we will eventually want to use a FF of the AMBER[47] family. However, since AMBER has been specially designed for amino acids, it is not well-suited to the present complexes. Consequently, for this "proof of concept" study, we use the general purpose Merck Molecular Force Field (MMFF),[48–51] which has a much richer set of atom types. In many respects, MMFF is similar to MM3,[52–54] which has been used as starting point for other attempts to design transition-metal-capable FFs in the past.[55] The insights gained here can then be transferred to other LFMM/FF combinations. Past experience has shown that no major problems are to be expected when using LFMM parameters evaluated and refined with MMFF in combination with AMBER.[12,13] Given that the LFMM core parameter set, namely the AOM-related part, is derived completely independently of the FF this observation is not surprising.

3. Computational Details

All LFMM calculations in this paper are carried out using our implementation of LFMM in the Molecular Operating Environment (MOE)[41,56] employing the MMFF94[48–51] FF. The FF was used without applying partial charges which were in any case found not to have a significant influence on the geometry. The AOM parameters and the ligand−ligand repulsion parameters for nitrogen ligands were taken from our library; the Morse parameters were adapted to the bonding situation in the chelate ligand. The AOM parameters

(45) Gerloch, M. *Magnetism and Ligand Field Theory*; Cambridge University Press: Cambridge, 1983.
(46) Gerloch, M.; McMeeking, R. F. *Dalton Trans.* **1975**, 2443–2451.
(47) Cornell, W. D.; Cieplk, P.; Bayly, C. I.; Gould, I. R.; Merz, J. K. M.; Ferguson, D. M.; Spellmeyer, D. C.; Fox, T.; Caldwell, J. W.; Kollman, P. A. *J. Am. Chem. Soc.* **1995**, *117*, 5179–5197.
(48) Halgren, T. A. *J. Comput. Chem.* **1996**, *17*, 490–519.
(49) Halgren, T. A. *J. Comput. Chem.* **1996**, *17*, 520–552.
(50) Halgren, T. A. *J. Comput. Chem.* **1996**, *17*, 553–586.
(51) Halgren, T. A.; Nachbar, R. B. *J. Comput. Chem.* **1996**, *17*, 587–615.
(52) Allinger, N. L.; Yuh, Y. H.; Lii, J.-H. *J. Am. Chem. Soc.* **1989**, *111*, 8551–8566.
(53) Lii, J.-H.; Allinger, N. L. *J. Am. Chem. Soc.* **1989**, *111*, 8566–8575.
(54) Lii, J.-H.; Allinger, N. L. *J. Am. Chem. Soc.* **1989**, *111*, 8576–8582.
(55) Wolohan, P.; Yoo, J.; Welch, M. J.; Reichert, D. E. *J. Med. Chem.* **2005**, *48*, 5561–5569.
(56) MOE 2006, Chemical Computing Group, 2006.

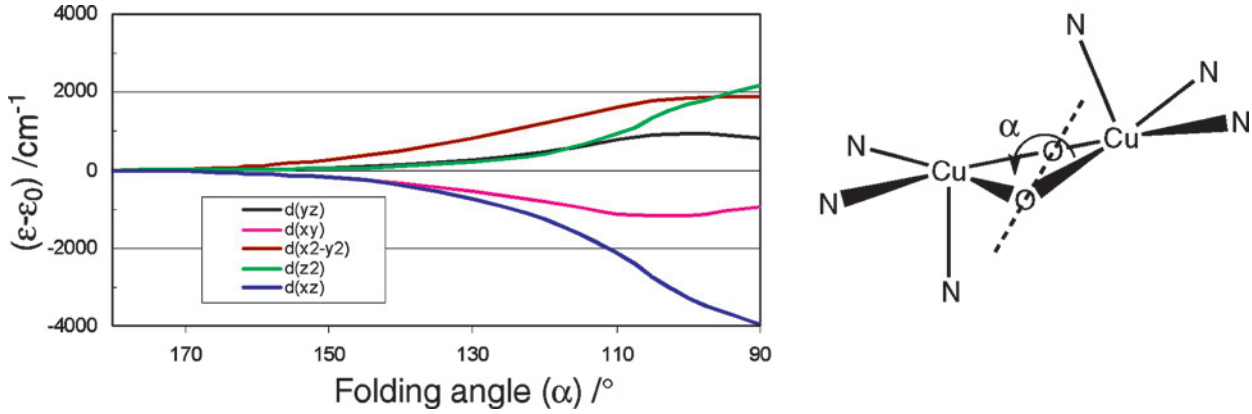

Figure 11. Variation of d orbital energy as a function of folding angle, α, of PO. α is defined on the right. Each d orbital energy, ϵ, is adjusted to zero by subtracting its actual energy, ϵ_0, at α =180°.

for the O_2^{2-} bridging ligand were derived as described above. The corresponding ligand−ligand repulsion and Morse parameters were initially obtained using the DFT geometry of PO as a reference. However, because of the general DFT tendency to overestimate the Cu−O bond lengths, the Morse parameters had to be slightly adjusted.

As a result of the antiferromagnetically coupled singlet ground state of the $[Cu_2O_2]^{2+}$ unit, all the compounds investigated in this work are subject to nondynamic correlation effects. It has been very nicely shown in ref 28 that within the framework of DFT (that is, if higher level methods are prohibited because the systems of interest are too large) the best way of dealing with this is to use pure DFT functionals as they tend to provide a reasonably balanced description of dynamic and nondynamic correlation for the molecules studies here.[28] Broken symmetry solutions of the Kohn–Sham equations using hybrid functionals like B3LYP seem not to be advisable,[28] and for pure DFT functionals, the solution is stable with respect to symmetry breaking anyway.[28,57] For these reasons, the BP86 gradient-corrected exchange correlation functional[58,59] was used throughout this paper.

All DFT geometry optimizations were carried out with the ridft module of the TURBOMOLE 5.7 program package.[60] The Coulomb integrals were approximated using the resolution of the identity approximation[61] utilizing the auxiliary basis sets from the TURBOMOLE basis set library.[62] The geometry of compound **Ia** was optimized using a triple-ζ valence basis set TZV(d,p)[63] on all atoms and was practically identical to that obtained using a TZV(d,p) basis set only on the copper atoms and a split valence (SVP)[64] one on all other atoms. The latter has therefore been used throughout this work. For the average over configurations calculations (see section 2.2.3) the Amsterdam Density Functional (ADF) package[65] was used, employing the valence triple-ζ (TZP) frozen core[66] (1s−2p on copper and 1s on O and N) basis sets from the ADF library for all atoms.

4. Results

Five-coordinate Cu(II) complexes are known for their great flexibility; hence, small energy perturbations may lead to large structural variations. For example, previous applications of the LFMM[14,67] give a small energy difference between square-pyramidal and trigonal-bipyramidal structures, but for Cu(II) species, these structures are associated with bond length changes of several tenths of an angstrom. In bigger molecules, we expect a comparatively large number of conformers to be accessible at room temperature. These issues are exacerbated for dinuclear Cu(II) complexes. Consequently, care has to be taken when comparing crystallographic structures with FF and DFT geometries from calculations on isolated molecules since, although the structures may appear distinctly different, their energies may be similar and possibly within the range of crystal packing effects. Therefore, for all four model compounds, extensive stochastic conformational searches have been carried out. The respective lowest energy structures were then reoptimized using DFT. Geometries with an LFMM energy of more than 3 kcal/

(57) Metz, M.; Solomon, E. I. *J. Am. Chem. Soc.* **2001**, *123*, 4938–4950.
(58) Becke, A. D. *Phys. Rev. A* **1988**, *38*, 3098–3100.
(59) Perdew, J. P. *Phys. Rev. B* **1986**, *33*, 8822–8824.
(60) TURBOMOLE (Vers. 5.7):Ahlrichs, R.; Bär, M.; Baron, H.-P.; Bauernschmitt, R.; Böcker, S.; Ehrig, M.; Eichkorn, K.; Elliott, S.; Furche, F.; Haase, F.; Häser, M.; Horn, H.; Huber, C.; Huniar, U.; Kattannek, M.; Kölmel, C.; Kollwitz, M.; May, K.; Ochsenfeld, C.; Ohm, H.; Schäfer, A.; Schneider, U.; Treutler, O.; von Arnim, M.; Weigend, F.; Weis P.; Weiss, H. Universität Karlsruhe, 2005.
(61) Eichkorn, K. O. T.; Ohm, H.; Häser, M.; Ahlrichs, R. *Chem. Phys. Lett.* **1995**, *242*, 652–660.
(62) Eichkorn, K.; Weigend, F.; Treutler, O.; Ahlrichs, R. *Theor. Chim. Acta* **1997**, *97*, 119–124.
(63) Schäfer, A.; Huber, C.; Ahlrichs, R. *J. Chem. Phys.* **1994**, *100*, 5829–5835.
(64) Schäfer, A.; Horn, H.; Ahlrichs, R. *J. Chem. Phys.* **1992**, *97*, 2571–2577.
(65) ADF (Vers. 2006.01):Baerends, E. J.; Autschbach, J.; Bérces, A.; Bickelhaupt, F. M.; Bo, C.; de Boeij, P. L.; Boerrigter, P. M.; Cavallo, L.; Chong, D. P.; Deng, L.; Dickson, R. M.; Ellis, D. E.; Fan, L.; Fischer, T. H.; Fonseca Guerra, C.; van Gisbergen, S. J. A.; Groeneveld, J. A.; Gritsenko, O. V.; Grüning, M.; Harris, F. E.; van den Hoek, P.; Jacob, C. R.; Jacobsen, H.; Jensen, L.; van Kessel, G.; Kootstra, F.; van Lenthe, E.; McCormack, D. A.; Michalak, A.; Neugebauer, J.; Osinga, V. P.; Patchkovskii, S.; Philipsen, P. H. T.; Post, D.; Pye, C. C.; Ravenek, W.; Ros, P.; Schipper, P. R. T.; Schreckenbach, G.; Snijders, J. G.; Sola, M.; Swart, M.; Swerhone, D.; te Velde, G.; Vernooijs, P.; Versluis, L.; Visscher, L.; Visser, O.; Wang, F.; Wesolowski, T. A.; van Wezenbeek, E.; Wiesenekker, G.; Wolff, S. K.; Woo, T. K.; Yakovlev, A. L. and Ziegler, T. Free University Amsterdam, Amsterdam, 2006.
(66) Baerends, E. J.; Ellis, D. E.; Ros, P. *Theor. Chim. Acta* **1972**, *27*, 339–354.
(67) Deeth, R. J.; Hearnshaw, L. A. *J. Chem. Soc., Dalton Trans.* **2005**, 3638–3645.

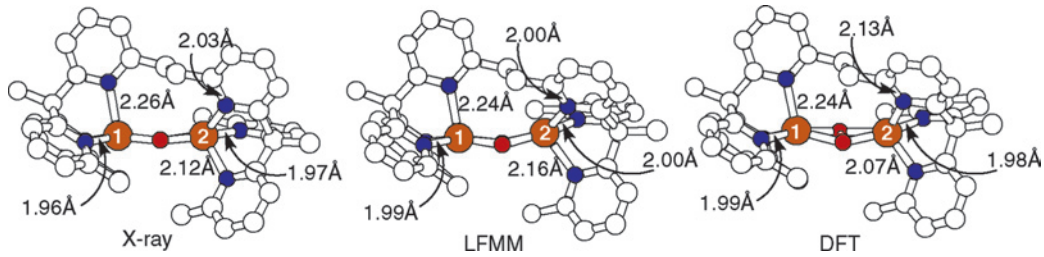

Figure 12. Observed X-ray structure (left), LFMM-computed structure (center), and DFT-optimized geometry (right) for **Ia** showing Cu−N distances. All comparable structural data for the X-ray and LFMM versions of **IIa** are virtually the same. H atoms are omitted for clarity.

Table 5. Comparison of Experimental, DFT, and LFMM Geometries for Compounds **I** and **II** (See Figure 12)

		experiment[a]		DFT[b]		LFMM	
	atoms	R^c	$\angle^d$	R^c	$\angle^d$	R^c	$\angle^d$
Ia	Cu1−N3	2.12	−61.1	2.07	−44.5	2.16	−66.6
	Cu2−N6	2.26	−74.5	2.20	−67.8	2.24	−71.5
	Cu1−N1, Cu1−N2	2.03, 1.97	34.7, 1.5	2.13, 1.98	51.0, 1.8	2.00, 2.00	24.5, 4.5
	Cu2−N4, Cu2−N5	1.97, 1.96	11.6, 9.7	1.98, 2.02	3.6, 26.5	1.99, 1.97	13.2, 10.7
	Cu1−O1, Cu1−O2	1.90, 1.96		1.96, 2.10		1.93, 1.93	
	Cu2−O1, Cu2−O2	1.91, 1.92		2.06, 1.96		1.92, 1.94	
	rel energy [kcal/mol]			0.0		0.0	
IIa	Cu1−N3	2.14	−59.7	2.07	−36.7	2.19	−66.5
	Cu2−N6	2.27	−72.9	2.25	−68.5	2.26	−72.5
	Cu1−N1, Cu1−N2	2.04, 1.98	35.0, 5.1	2.20, 2.00	57.4, 1.1,	2.01, 2.01	24.6, 5.3
	Cu2−N4, Cu2−N5	1.97, 1.99	5.8, 17.7	2.00, 2.04	2.6, 25.1	2.00, 1.99	7.8, 14.8
	Cu1−O1, Cu1−O2	1.91, 1.92		1.97, 2.06		1.93, 1.93	
	Cu2−O1, Cu2−O2	1.89, 1.91		2.04, 1.97		1.92, 1.93	
	rel energy [kcal/mol]			0.0		0.0	
Ib	Cu(1, 2)−N_{ax}			2.17	−60.0	2.21	−63.1
	Cu(1, 2)−N_{eq}			2.04, 1.98	35.2, 0.3	2.00, 1.98	26.1, 1.1
	Cu(1, 2)−O			1.96, 2.08		1.93, 1.94	
	rel energy [kcal/mol]			0.0		0.9	
IIb	Cu(1, 2)−N_{ax}			2.23	−63.3	2.24	−68.2
	Cu(1, 2) - N_{eq}			2.05, 2.00	30.7, 0.4	2.02, 2.00	21.6, 3.1
	Cu(1, 2) - O		1.97, 2.05			1.93, 1.94	
	rel energy [kcal/mol]			0.0		0.2	
Ic	Cu(1, 2) - N_{ax}			2.17	−69.5	2.21	−71.1
	Cu(1, 2) - N_{eq}			2.03, 1.99	27.9, 3.8	1.99, 2.00	21.3, 3.6
	Cu(1, 2)−O		1.95, 2.15			1.95, 1.94	
	rel energy [kcal/mol]			2.3		1.8	
IIc	Cu(1, 2)−N_{ax}			2.24	−72.7	2.25	−72.9
	Cu(1, 2)−N_{eq}			2.04, 2.02	21.4, 6.4	2.02, 2.02	13.2, 10.6
	Cu(1, 2)−O		1.96, 2.11			1.95, 1.94	
	rel energy [kcal/mol]			3.6		2.4	

[a] References 23 and 24. [b] Technical details in computational details section. [c] Bond lengths (in Å) between atoms given in first column. [d] Angles (in deg) between CuOO plane and bond vectors of atoms given in first column.

mol above the lowest conformer—corresponding to a Boltzmann weight of less than 1% at room temperature—were not considered further except for compound **IV** as detailed later.

4.1. Pyridyl Chelate Ligands. As mentioned in the Introduction, the crystal structures of **I** and **II** are quite similar. Both suggest an asymmetric lowest energy conformer (**Ia** and **IIa**) in which the J−T axes of the two metal centers are on different sides of the $[Cu_2O_2]^{2+}$ pseudoplane. Because of the ethylene bridge connecting the two tridentate donor units, the two copper centers have significantly different environments. The tetragonal elongation of the axial ligand on Cu2 (see Figure 12) is less pronounced and the coordination is tetrahedrally distorted, whereas Cu1 has a more regular square-pyramidal geometry with the equatorial ligands nearly in the Cu−peroxido plane (see Figure 12 and Table 5). The LFMM stochastic conformational search gives the crystal structure conformation as the energetically favored one. The DFT structure of **Ia** is also fairly similar to the other two but has twisted both the CuN_3 moieties on Cu1 and Cu2 relative to the Cu−peroxido plane and also alters the sense of the J−T elongation on Cu2. The latter is even more pronounced for **IIa** where DFT now further lengthens the longer Cu−N contact on Cu2 from 2.13 Å in **Ia** to 2.20 Å in **IIa**.

For both compounds **I** and **II**, two further C_2 symmetric conformers are found by LFMM. The respective lower energy ones of these conformers (**Ib** and **IIb**, see Table 5) are energetically very close (0.9 and 0.2 kcal/mol) to the minima obtained when optimizing from the crystal structure. The geometries of the higher energy conformers (**Ic** and **IIc**) are also quite similar to **Ib** and **IIb**. They only differ by the twisting angle between the two sides of the chelate ligand with respect to each other, which results in a different arrangement of the bridging ethylene units (see Figure 13).

DFT optimizations starting from the LFMM structures of the higher energy systems yield very similar local minima (see Table 5) although, as for **Ia** and **IIa**, DFT gives a slightly more asymmetric binding mode than

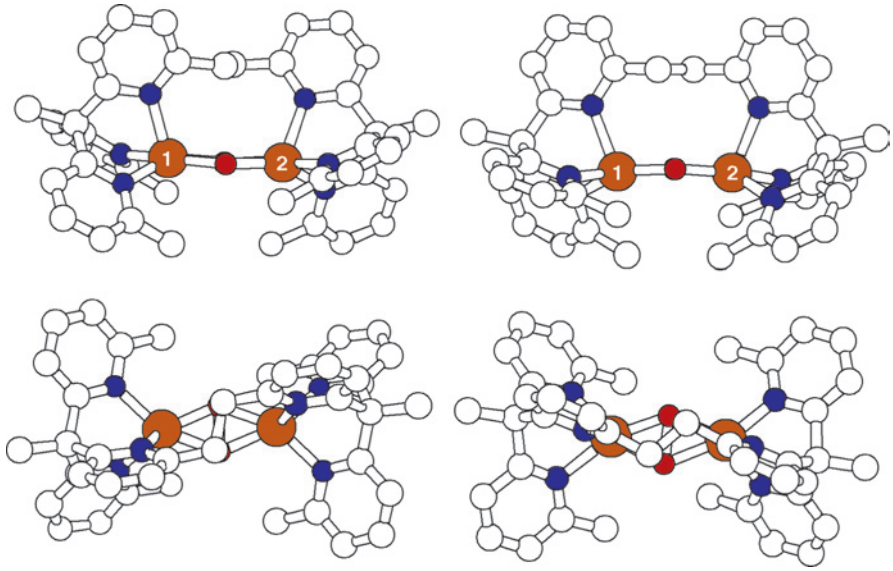

Figure 13. LFMM geometries of **Ib** (left-hand side) and **Ic** (**IIb** and **IIc** very similar). Top: view down O−O vector. Bottom: view perpendicular to the $[Cu_2O_2]^{2+}$ plane.

Table 6. Comparison of Experimental, DFT, and LFMM Geometries for Compound **III** (See Figure 2)

	experiment[a]		DFT[b]		LFMM	
atoms	R^c	$\angle^d$	R^c	$\angle^d$	R^c	$\angle^d$
$Cu-N_{ax}$	2.26	−65.0	2.28	−66.2	2.21	−74.0
$Cu-N_{eq}$	1.99,2.00	17.4, 12.0	2.00, 2.00	16.1, 14.1	2.01, 2.02	11.4, 11.1
Cu−O	1.90,1.93		2.00, 2.00		1.94, 1.94	

[a] References 25 and 26. [b] Technical details in computational details section. [c] Bond lengths (in Å) between atoms given in first column. [d] Angles (in deg) between CuOO plane and bond vectors of atoms given in first column.

LFMM. The experimental structures of **Ia** and **IIa** do not show this distortion and thus agree with LFMM. The DFT results might be affected by their inherent shortcomings (see section 2). However, the energetic balance here is very subtle since the "incorrect" lowest energy structures of **Ia** and **IIa** from DFT correspond more-or-less to LFMM structures **Ib** and **IIb**. The energy differences are probably smaller than the uncertainties in the calculations. The "failure" of DFT to reproduce the correct orientation of the J−T axis for **Ia** and **IIa** and the rather more distorted geometry than experimentally found is probably not significant although, interestingly, despite the apparent similarity of the two systems, the error is more severe in the case of **IIa**. As mentioned in the Introduction, this shows that the balanced description of the strain within the ligand on the one hand and the J−T distortion on the other hand represents a theoretically demanding task. The remarkable agreement between the LFMM and experimental geometries for **Ia** and **IIa** is thus even more noticeable.

For the higher energy conformers **Ib**, **Ic**, **IIb**, and **IIc**, for which no experimental data are available, the orientation and order of magnitude of our main quantity of interest, namely the J−T distortion, agree very well between DFT and LFMM. Even though DFT appears to be slightly less reliable for these compounds, the fact that two entirely different methods largely agree about the structural features of **Ib**, **Ic**, **IIb**, and **IIc** gives us some confidence that the predictions are correct.

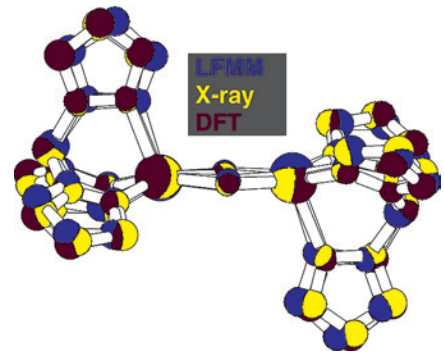

Figure 14. Overlaid structures of **III**. Hydrogen and isopropyl groups are omitted for clarity.

4.2. Tris(pyrazolyl) Borate Ligand. For **III** no conformers other then the experimentally found one were obtained. This is not surprising since the orientation of the ligand atoms is very close to ideal (see Table 6), and the isopropyl groups of the two ligands mesh tightly such that conformational changes are accompanied by a high-energy penalty. The very symmetric binding mode of the peroxido unit is reproduced by DFT and LFMM (Figure 14). Just as for compounds **I** and **II**, DFT tends to slightly overestimate the Cu−O bond lengths.

The structure of **III** is the result of a balance between Pauli repulsion and dispersion attraction among the sterically demanding ligands on the one hand and the binding of the peroxido bridge on the other hand. This obviously is described very well by the LFMM. The somewhat worse performance of DFT could possibly be related to the lack of dispersion forces and the resulting overestimation of the Pauli

Table 7. Comparison of Experimental, DFT, and LFMM Geometries for Compound **IV** (See Figure 15)

		experiment[a]		DFT[b]		LFMM	
	atoms	R^c	$\angle^d$	R^c	$\angle^d$	R^c	$\angle^d$
IVa	Cu1−N3	2.22	−42.8	2.21	−27.3	2.13	−18.7
	Cu2−N6	2.22	−48.4	2.44	−64.7	2.32	−61.6
	Cu1−N1, Cu1−N2	1.99, 2.11	10.0, 43.5	2.05, 2.24	−16.3,58.1	2.03, 2.23	−17.8, 66.2
	Cu2−N4, Cu2−N5	2.10, 2.02	37.1, 3.9	2.09, 2.07	11.3, 6.4	2.08, 2.09	6.8, 14.3
	Cu1−O1, Cu1−O2	1.92, 1.96		2.04, 1.99		1.96, 1.97	
	Cu2−O1, Cu2−O2	1.89, 1.81		1.99, 2.01		1.96, 1.97	
	rel energy			0.0		0.0	
IVb	Cu1−N3			2.12	−22.2	2.25	−60.6
	Cu2−N6			2.27	−73.7	2.25	−72.7
	Cu1−N1, Cu1−N2			2.30, 2.09	55.3,-11.8	2.11, 2.05	24.2, 3.1
	Cu2−N4, Cu2−N5			2.11, 2.07	24.4, 2.4	2.07, 2.06	9.4, 13.9
	Cu1−O1, Cu1−O2			2.00, 2.00		1.96, 1.95	
	Cu2−O1, Cu2−O2			1.99, 2.03		1.96, 1.95	
	rel energy			+2.4		−10.0	
IVc	Cu1−N3			2.28	−71.0	2.25	−73.7
	Cu2−N6			2.28	−71.1	2.25	−73.7
	Cu1−N1, Cu1−N2			2.09, 2.10	10.8, 20.3	2.06, 2.08	15.0, 10.6
	Cu2−N4, Cu2−N5			2.10, 2.09	21.0, 10.3	2.08, 2.06	10.7, 15.0
	Cu1−O1, Cu1−O2			2.09, 1.95		1.95, 1.96	
	Cu2−O1, Cu2−O2			1.95, 2.09		1.96, 1.95	
	rel energy			+3.1		−9.5	

[a] Reference 27. [b] Technical details in computational details section. [c] Bond lengths (in Å) between atoms given in first column. [d] Angles (in deg) between CuOO plane and bond vectors of atoms given in first column.

repulsion between the ligands which leads to an elongation of the Cu−O bonds.

4.3. Triazacyclodecane Macrocycle Ligand. Compound **IV** is by far the theoretically most demanding. The combination of the "soft" J−T distorted Cu centers and the rather more flexible iPr_3TACDD ligands (TACDD = 1,5,9-triazacyclodecane) gives rise to a variety of conformers which are potentially similar in energy. The main differences among these conformers are the orientation of the two chelate ligands with respect to each other and the relative orientation of the J−T axes of the two metal centers. Furthermore, the five-membered Cu(en) rings can take on two different but energetically similar conformations, and there are many relatively similar but distinguishable ways that the sterically demanding isopropyl groups of the two ligands mesh. As evident from the QM/MM calculations in ref 27, the interactions between the iPr groups at the same time have an important influence on the geometry around the metal centers.

In light of these considerations, it appears somewhat surprising that the LFMM conformational search only yields two different conformers for **IV** in the range of 3 kcal/mol—none of which is related to the experimentally found structure (see Table 7). The lowest energy conformer (**IVb**) on the LFMM potential energy hypersurface is shown in Figure 15 (bottom left). It is characterized by the two J−T elongated bonds (shown in gray in Figure 15) being on the same side of the $[Cu_2O_2]^{2+}$ pseudoplane in a cis-like arrangement. The axial position is occupied by one of the "asymmetric" nitrogen atoms of the iPr_3TACDD ligand which is bound to one ethylene and the propylene bridge (the latter highlighted in light blue in Figure 15). The corresponding trans form with the J−T elongated bonds on opposite sides represents the second conformer in the 3 kcal/mol range (**IVc**). DFT yields a very similar geometry for the trans structure but gives a somewhat "less symmetric" structure for the cis conformer.

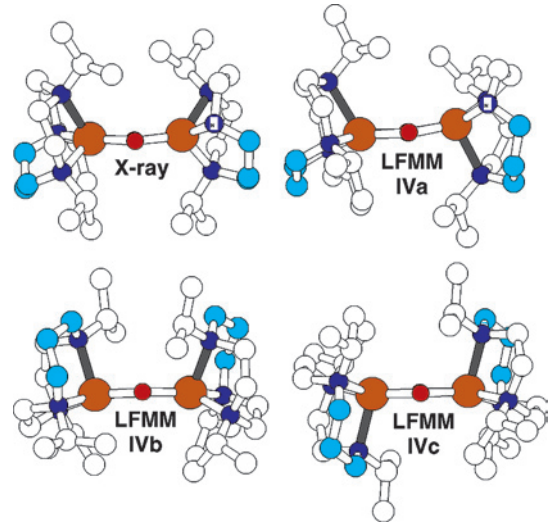

Figure 15. Comparison of X-ray structure of **IV** with the three LFMM structures. The longest Cu−N distances for each Cu center are shown in gray, and the C_3 chains of the propylene units are highlighted in light blue.

LFMM optimization starting from the experimental geometry results in a local minimum which is very similar to the corresponding DFT structure and in reasonable agreement with the crystal structure. The important difference between the latter and the two computational structures is the orientation of the peroxido bridge with respect to the nitrogen ligand atoms. In the experimental geometry, the coordination spheres of the two copper atoms are very similar, whereas DFT and LFMM predict a slightly different arrangement of the peroxido bridge which imposes a stronger tetragonal distortion on Cu2 and a somewhat more tetrahedral geometry on Cu1. This is apparent in the angles between the Cu−peroxido plane and the Cu−N binding axes summarized

Table 8. Contributions to the LFMM Energy for **IV**

contribution	**IVa**	**IVb**	**IVc**
LFSE	−83.5	−89.2	−89.7
ligand−ligand repulsion	+88.9	+91.9	+90.9
Morse potential	−570.6	−572.8	−572.9
MMFF94	+409.3	+404.0	+406.2
total	−156.0	−166.0	−165.5

in Table 7 although the way these angles are defined (9) tends to accentuate what is actually a relatively small difference in overall structure.

However, the fact that DFT and LFMM yield very similar structures suggests that the difference with respect to experiment either originates from a subtle electronic effect which can be captured neither by DFT nor by LFMM or, more likely, is partly the result of crystal packing effects. However, more importantly than the error in the geometry, LFMM yields an energy for the local minimum obtained by using the experimental structure as a starting point which is ≈10 kcal/mol higher than the lowest energy conformers found by the conformational search (**IVb/IVc**). Given the excellent performance of the LFMM for the other three compounds, this deviation needs careful analysis.

Remarkably, and in contrast to our findings for **I** and **II**, the relative DFT energies (see Table 7) differ substantially from the LFMM ones. At the DFT level, **IVa** is correctly predicted to be lower in energy than **IVb** and **IVc**. However, the relative energies of the latter agree with the LFMM. Unfortunately, there are ≈90 conformers in the energetic range between 0 and 12 kcal/mol such that an analysis with DFT is impractical. Therefore, we will try to examine the problem by carefully inspecting the geometries of **IVa**−**IVc** and the individual contributions to the LFMM energy (see Table 8).

Evidently, the energy difference between **IVa** and **IVb/IVc** is mainly due to the LFSE and the conventional FF contribution. In this context two points are important to mention: the most striking difference between the conformers is the respective orientation of the hydrocarbon bridges in the chelate ligands (ethylene and propylene) and the J−T elongated N−Cu bond. As mentioned above, in **IVb/IVc** this bond corresponds to one of the "asymmetric" nitrogens bound to one ethylene and the propylene bridge. Experimentally, the asymmetric nitrogens on both copper sites occupy the pseudoequatorial positions. This implies that there are deficiencies in the LFMM (in combination with MMFF94) regarding the balanced description of five-membered Cu(en) rings relative to six-membered Cu(pn) rings and the resulting strain within the chelate ligand. The second important point is that despite the apparently wrong energy, the geometry of **IVa** is reasonably close to the experimental one. The incorrect orientation of the J−T axis found with LFMM is present in the DFT structure as well, and the discrepancy with experiment might very well be a crystal packing effect.

Since the LFSE seemingly incorrectly favors the "wrong" conformers **IVb** and **IVc** (see Table 8), an exhaustive reparametrization study has been conducted to obtain the correct energetics for **IV** while retaining the excellent performance for **I**−**III**. However, in the course of this study it became clear that the error has to be attributed to the FF to a large extent. Even with the AOM treatment turned off the energy difference between **IVa** and **IVb** is still 6.5 kcal/mol in favor of **IVb**, all of which is due to the FF contribution. Furthermore, qualitatively speaking, the LFMM structure of **IVa** looks "more distorted" in the sense that it deviates more from the "unstrained" $(NH_3)_3Cu_2O_2(NH_3)_3]^{2+}$ arrangement given in PO than **IVb**. By chemical intuition **IVa** therefore has to have a less negative LFSE, and the energetics have to be "fixed" by the conventional FF terms. This suggests that MMFF is not properly describing the macrocycle ligand irrespective of whether it is coordinated to a metal or not.

Table 9. Energy Differences between Optimized Ligand Conformers of **IVa** and **IVb** (See Text)

method	E(**IVa** − **IVb**)/kcal/mol
MMFF94[a]	+10.0
MMFF94 vdW contrib	+0.8
MM3[a]	+9.2
DFT(BP86/SVP)[b]	−1.2

[a] Electrostatic contribution is small (numbers presented are without charges). [b] BP86/TZVP essentially identical. Energy differences between optimized ligand conformers of **IVa** and **IVb** (see text).

In order to substantiate this somewhat tentative reasoning, we carried out geometry optimizations of the ligands starting from their respective conformations in the metal complex. This was done for **IVa** (minimum from X-ray crystallography and DFT) and for **IVb** (LFMM minimum structure from stochastic search). The results are summarized in Table 9. Obviously, even though the geometries were allowed to relax, MMFF94 (as well as MM3 which has been additionally included for comparison) strongly favors the macrocycle conformations present in the LFMM minimum structure. This is in contradiction with DFT, which predicts the conformers to be almost isoenergetic. Given the vanishingly small vdW contribution to the relative energy (estimated on the basis of the MMFF vdW terms), the DFT numbers can be regarded as relatively reliable here. This finding strongly supports our hypothesis that the wrong energetic ordering of **IVa** and **IVb/IVc** is not related to the LFMM treatment but should rather be attributed to shortcomings in the FF. Given the unusual ring size of the macrocycle and the resulting "nonstandard" bond and torsion angles, this probably it not as surprising as it might first appear. It is, however, important to note that the observed problem is special to the macrocycle ligand used in **IV** and will not be relevant for the description of the T3 center in an actual protein environment using AMBER as the parent FF.

4.4. Cu−O and O−O Distances. For each CuO_2 fragment, the data presented often show DFT generating unequal Cu−O distances while experiment and LFMM give virtually equal distances. In contrast, for the O−O distances (Table 10), it is now DFT and LFMM which agree with each other with a different trend found experimentally.

We expected only minor variations in LFMM O−O distances since there is very little apart from the dominant bond stretch potential which might affect the O−O bond, and yet DFT gives a similar result. LFMM thus combines the symmetry in the Cu−O distances observed experimen-

Table 10. O−O Bond Lengths (Å)[a]

compound	X-ray	DFT	LFMM
I	1.49	1.44	1.45
II	1.49	1.44	1.45
III	1.41	1.44	1.46
IV	1.37	1.46	1.44

[a] Computed data refer to isomer "a" where appropriate.

tally with the constant O−O bond length found with DFT. The O−O vibrational frequency would be expected to correlate with the O−O distance and might resolve the issue of which result is correct. However, we do not pursue this further since the current LFMM treatment would not be sufficiently accurate to differentiate subtle spectroscopic differences while the calculated asymmetry in the Cu−O distances may make DFT calculations of dubious worth.

Finally, although the model implicitly gives a flat $[Cu_2O_2]^{2+}$ unit, we still see in **I** (Figure 12) and **IV** (Figure 15) the same type of "butterfly" or folding distortion observed in T3 enzyme active sites. This gives us some confidence that, once ported to the AMBER FF, the present LFMM treatment will provide a sound basis for modeling complete T3 metalloproteins.

5. Conclusion

This work represents the first application of ligand field molecular mechanics (LFMM) to dinuclear transition metal complexes. We have shown that, at least in the case of the $[Cu_2O_2]^{2+}$ cluster present in the model compounds considered in this paper, a purely local treatment of the metal centers without explicitly incorporating metal−metal coupling into the model is sufficient to reproduce the structural features. There is good reason to believe that this also holds for the active sites in T3 enzymes which are structurally very similar. A crucial aspect of the LFMM treatment, however, is the explicit need for AOM parameters describing the Cu−O π interactions. On the bais of DFT and ligand field calculations on the model mononuclear system $[Cu(O_2)(NH_3)_3]$, we established that the in-plane π parameters needed to be substantially larger than those describing π interactions perpendicular to the CuO_2 plane. For dinuclear complexes, overall planarity of the $[Cu_2O_2]^{2+}$ moiety is achieved by defining each local Cu−O axis frame using the other copper center rather than the other oxygen.

The performance of the method was evaluated on the basis of a set of four model compounds for the T3 center for which X-ray structures are available. For all four model compounds the LFMM geometries obtained by using the crystal structures as starting points agree remarkably well with experiment. In order to evaluate the LFMM potential energy surface further away from the experimental minimum, we carried out exhaustive LFMM conformational searches. All structures within an energy range of 0–3 kcal/mol were optimized at the DFT (BP86/SVP) level of theory. For three out of the four compounds, the DFT structures and energies agree very well with the LFMM. The outlier (**IV**) has a LFMM minimum-energy structure some 10 kcal mol^{-1} lower than that for the structure which is in best agreement with experiment.

Compound **IV** has therefore been carefully analyzed. The energetic differences can be mainly attributed to FF deficiencies with MMFF (and MM3) favoring the wrong macrocycle conformation. However, this problem is restricted to iPr_3TACDD (TACDD = 1,5,9-triazacycododecane) and will not hinder our goal of porting the LFMM parameters to the AMBER FF and applying the method to T3 enzymes.

In summary, we have shown that the LFMM in its present form provides the flexibility to describe the copper type 3 site in metalloproteins with at least the same accuracy as the DFT part in a QM/MM approach but at a fraction of the computational cost. This study suggests that LFMM represents a valuable tool for the analysis of the time-dependent behavior of copper type 3 enzymes by means of molecular dynamics simulations. This will be the subject of future work.

Acknowledgment. This work was supported by the German Academic Exchange Service (DAAD) and the biotechnology and biological science research council (BBSRC) of the UK. The authors also thank the National Service for Computational Chemistry Software (NSCCS) for providing computing time. The use of the EPSRC's Chemical Database Service at Daresbury is also gratefully acknowledged.[68]

Supporting Information Available: DFT and LFMM optimized geometries available. This material is available free of charge via the Internet at http://pubs.acs.org.

IC701803G

(68) Fletcher, D. A.; McMeeking, R. F.; Parkin, D. *J. Chem. Inf. Comput. Sci.* **1996**, *36*, 746–749.